PCCP

Ionic liquid based lithium battery electrolytes: Fundamental benefits of utilizing both TFSI and FSI anions?

Journal:	*Physical Chemistry Chemical Physics*
Manuscript ID:	CP-ART-03-2015-001891.R1
Article Type:	Paper
Date Submitted by the Author:	26-May-2015
Complete List of Authors:	Kerner, Manfred; Chalmers University of Technology, Applied Physics Plylahan, Nareerat; Chalmers University of Technology, Applied Physics Scheers, Johan; Chalmers University of Technology, Applied Physics Johansson, Patrik; Chalmers University of Technology, Applied Physics

PCCP

ARTICLE

Ionic liquid based lithium battery electrolytes: Fundamental benefits of utilising both TFSI and FSI anions?

Received 00th January 20xx,
Accepted 00th January 20xx

DOI: 10.1039/x0xx00000x

www.rsc.org/

M. Kerner,*[a] N. Plylahan,[a] J. Scheers[a] and P. Johansson[a,b]

Several IL based electrolytes with an imidazolium cation (EMI) have been investigated trying to elucidate a possible beneficial effect of mixing FSI and TFSI anions in terms of physico-chemical properties and especially Li^+ solvation. All electrolytes are evaluated in terms of phase transitions, densities and viscosities, thermal stabilities, ionic conductivities and local structure, i.e. charge carriers. The electrolytes with up to 20 % of Li-salts showed to be promising for high temperature lithium ion battery application (*ca.* 100°C) and a synergetic effect of having mixed anions is discernible with the $LiTFSI_{0.2}EMIFSI_{0.8}$ electrolyte giving the best overall performance. The determination of the charge carriers revealed the SN to be *ca.* 2 for all analysed electrolytes, and proved the analysis of the mixed anion electrolytes to be challenging and inherently leads to an ambiguous picture of the Li^+ solvation.

1. Introduction

The high specific energy density of lithium ion batteries (LIBs) makes them the battery technology of choice for many applications [1, 2]. The electrolytes of conventional LIBs, however, contain both organic volatile solvents and salts with anions prone to decompose, limiting their application to temperatures around ambient, often restricted to lower than *ca.* 60°C [3]. A possible alternative for high temperature LIBs "HT-LIBs" (operating > 60°C) applications are ionic liquid (IL) based electrolytes; they have a general set of properties of wide liquid range, low vapour pressure, thermally stable, and are often considered non-flammable [4-6]. In addition they can be electrochemically stable over a wide potential range and have high ionic conductivities [5], especially at high temperatures [7].

The number of possible ILs has been estimated to be extremely large; > 10^{12} or even much larger [8, 9], which makes it possible to tailor ILs for specific applications. This variety has been made use of in electrolytes, where cations of the imidazolium (XMI), piperidinium (PIP), pyrrolidinium (Pyr_{xy}) families, *etc.* have been combined with anions such as bis(fluorosulfonyl)imide (FSI), bis(trifluoromethanesulfonyl)imide (TFSI) and hexafluorophosphate (PF_6^-) [10-13]. For LIBs the ILs are most often mixed with the corresponding Li-salt *e.g.* LiTFSI. As one example utilising such electrolytes Seki *et al.* showed a LIB with a charge/discharge capacity of 300 mAh g^{-1} at room-temperature with a $Li_xPyr_{13(1-x)}TFSI$ electrolyte [14]. In terms of cycling stability, Garcia *et al.* demonstrated a battery with a 1M LiTFSI in EMITFSI electrolyte outperforming a 1M LiTFSI in EC:DMC electrolyte at a rate of 1C for 200 cycles [11].

IL based electrolytes can be modified into hybrid electrolytes [15], by adding organic solvents, to improve the ion transport and interfacial properties [16, 17] - but at the risk of losing the IL safety features at higher temperatures [18]. Another trend is to add a Li-salt with a different anion than in the IL [19, 20]. Replacing TFSI by FSI, or combining the two, has been motivated by enhanced ionic conductivities [19] and improved passivation of the aluminium current collector [21]. The primary drawback is the risk of a lower thermal stability [22]; exemplified by the temperature for 5 % weight loss of the ILs EMITFSI (374°C) and EMIFSI (225°C) [23]. Lahiri *et al.* very recently showed a superior behaviour of a battery with an $LiTFSI_xPyr_{14}FSI_{(1-x)}$ electrolyte as compared to an $Li_xPyr_{14(1-x)}TFSI$ electrolyte with respect to capacity and stability [24]. Nádherná *et al.* successfully used $LiFSI_xPyr_{14}TFSI_{(1-x)}$ at 55°C (350-360 mAh g^{-1}) and Yamagata *et al.* $LiTFSI_xEMIFSI_{(1-x)}$ in a graphite half-cell at 60°C [25]. Furthermore, Yamagata *et al.* proposed an electrochemical double-layer structure to be created on the electrode surface instead of the in conventional electrolytes formed solid electrolyte interphase (SEI), protecting the EMI cation from decomposition, and thereby improving the cathodic stability [26]. The non-trivial nature of these double-layer structures together with their dependence not only on the electrolyte, but also on the electrode material was shown by Costa *et al.* [27]. Another advantage of an EMIFSI IL based system was elucidated by impedance spectroscopy; Sugimoto *et al.* found a much lower impedance for $LiTFSI_xEMIFSI_{1-x}$ as compared to LiTFSI in EC:DMC [28]. At higher temperatures, 80-120°C, the performance of IL based electrolytes seems complicated [29-32]. Yet, Matsumoto *et al.* reported stable cycling for different IL based electrolytes with LiTFSI at 85°C [29].

Combining the approaches above, we here investigate the physico-

[a] Department of Applied Physics, Chalmers University of Technology, SE-41296 Gothenburg, Sweden.
[b] Current position: Visiting Professor at LRCS/CNRS UMR7314, Université de Picardie Jules Verne, 33 rue Saint Leu, 80039 Amiens, France.

† Footnotes relating to the title and/or authors should appear here.
Electronic Supplementary Information (ESI) available: [details of any supplementary information available should be included here]. See DOI: 10.1039/x0xx00000x

chemical properties of IL based electrolytes with both FSI and TFSI aiming towards operating temperatures of *ca.* 100°C. EMIFSI and EMITFSI are combined with ≤ 20 mol% LiTFSI or LiFSI – giving four unique sets of electrolytes. For reference purposes the neat ILs are also studied. Focus is on thermal stabilities, phase transitions, and ionic conductivities. A detailed Raman spectroscopic analysis is performed to reveal the charge carriers in the electrolytes *i.e.* if there is a FSI or TFSI solvation preference of the Li^+ cation. Furthermore, the electrochemical stability window (ESW) is determined to elucidate the possible working range and hence possible suitable electrode materials.

2. Experimental

2.1 Sample preparation

The ILs 1-ethyl-3-methylimidazolium FSI, EMIFSI (99.9 %), and EMITFSI (99 %), were purchased from Solvionic and used as received. LiTFSI (99.95 %) and LiFSI (99.5 %) were purchased from Sigma-Aldrich and Suzhou Fluolyte, respectively. The Li-salts were dried for 72 h under vacuum (< 7 Pa) at 120°C and 80°C, respectively. Four families of electrolytes; $LiTFSI_xEMI(T)FSI_{(1-x)}$ and $LiFSI_xEMI(T)FSI_{(1-x)}$ were prepared by direct mixing of appropriate amounts of salt and IL to reach molar fractions of x=0.1 and 0.2. Thus, in total eight electrolytes were prepared. All materials were stored and handled in an argon filled glove box (H_2O < 1 ppm, O_2 < 1 ppm). EMIFSI and its electrolytes had < 100 ppm H_2O, while EMITFSI and its electrolytes had < 30 ppm H_2O, as measured by Karl Fischer titration (KF Coulometer, Metrohm).

2.2 Phase transitions and thermal stability

Differential scanning calorimetry (DSC) was performed using a Q1000 from TA instruments. *Ca* 10 mg of sample, in a hermetically sealed aluminium pan, was cooled to -150°C before heated up to 150°C, with 5 min equilibration time at the extreme temperatures. Stepwise, faster cooling rates of 5, 10, 20, and 40°C min^{-1} were used to suppress crystallization and promote the observation of the glass transitions, while a common heating rate of 5°C min^{-1} was used. The points of inflection of the transitions were used to determine the glass transition temperatures, T_g, while the onset of the endothermic peaks were used to determine the melting points, T_m. Thermal gravimetric analysis (TGA) was performed using a TG 209 F1 Iris from Netzsch. An alumina crucible was loaded with *ca.* 10 mg of sample and placed in the sample compartment where a nitrogen flow of 100 ml min^{-1} was applied. All samples were heated from 25°C to 500°C at a rate of 5°C min^{-1}. The decomposition temperatures (T_d) were defined as the temperature of 1% mass loss. In addition, isothermal TGA measurements were performed at 100°C and 125°C to study "long-term" stability, each temperature was maintained for 10 h.

2.3 Density and viscosity

The densities (ρ) and viscosities (η) were determined using a DMA 4500M density meter from Anton Paar with a Lovis 2000 M micro-viscometer module. A steel ball (Ø=1.5 mm, ρ=7.70 g cm^{-3}) was used for dynamic viscosity measurements by the falling sphere method. The capillaries (Ø=1.59 or 1.8 mm) were loaded inside the glove box. The densities and viscosities were recorded in 10°C steps from 20°C to 90°C and back to 20°C. The results from the cooling runs were used for all further analysis.

2.4 Ionic conductivity

The ionic conductivities (σ**)** were obtained by dielectric spectroscopy in the frequency range 10^{-1} – 10^{7} Hz with a broadband dielectric spectrometer (Concept 80, Novocontrol GmbH) with a Quattro Cryosystem temperature control unit. The sample cell, with blocking stainless steel electrodes, had an inner diameter, Ø = 13.3 mm, and a thickness, 1.04 mm, defined by a Teflon spacer. The cell was filled with sample inside the glove box and transferred to the instrument in a closed box. Starting at 20°C, the samples were heated to 150°C and then cooled to -110°C in 10°C steps, using a 30 min equilibration time before measurement at each temperature. The higher temperatures might cause minor leakage of electrolyte, but the measured volume is approximately constant. The DC conductivities were obtained from the plateaus of the frequency dependent (AC) conductivity plots for each temperature.

2.5 Ionic interactions and local coordination

Molecular level interactions were studied using a Bruker MultiRAM FT-Raman spectrometer with a Nd:YAG laser (1064 nm, 250 mW) and a spectral resolution of 2 cm^{-1}. Data were typically averaged over 1000 to 3000 scans and recorded as a function of temperature at 30, 60, 90, and 120°C. All samples were filled in an open aluminium pan and placed in a hermetically sealed Linkam FTIR600 temperature controlled stage filled with dry argon gas. For a detailed analysis of the region 680 - 790 cm^{-1}, $Li_xEMI_{1-x}FSI$ spectra were deconvoluted using Gaussian functions, while the $Li_xEMI_{1-x}TFSI$ spectra were deconvoluted using pseudo-Voigt functions (Gaussian:Lorentzian = 60:40), the latter following the procedure of Lassegues *et al.* [33]. Solvation numbers (SN) for the lithium cations were calculated from the deconvoluted spectra in accordance with the procedure of Pitawala *et al.* [34]; dividing the area of the band corresponding to Li^+ coordinated anions (A_C) with the total band area (including also the contributions from "free" anions (A_F)) and the molar fraction of Li-salt (x) (eq. 1).

$$SN = \frac{A_C/(A_F+A_C)}{x} \qquad (1)$$

To support the interpretation of the experimental spectra, artificial Raman spectra were created using data from density functional theory (DFT) calculations, (B3LYP/6-311+G(d)). The conductor-like polarizable continuum model (C-PCM) was used to account for the solvent [35]. The minimum energy conformers of both FSI and LiFSI ion-pairs, which have been discussed elsewhere [36], were geometry optimized using ACN as solvent (ε=35.7) for an improved description *vs.* a vacuum approach [37]. Second and third derivatives of the energies with respect to nuclei displacements were calculated to verify the structures as energy minima and to obtain the vibrational modes and the Raman activities. The calculated vibrational frequencies are reported without any scaling factor. All calculations were performed with the Gaussian09 software package [38].

2.6 Electrochemical stability window

In order to determine the electrochemical stability windows (ESW) of the electrolytes, linear sweep voltammetry (LSV) was performed using a 2-electrode Swagelok cell with stainless steel as working electrode and metallic Li-foil as counter/ reference electrode. A circular sheet of glass microfiber (∅ = 14 mm) was used as separator and soaked with 80 µl of the electrolyte. All cells were assembled inside the glovebox under Ar atmosphere. The LSV experiments were conducted with a scan rate of 0.5 mV s^{-1} using identical, but different, cells for the anodic scan, from open circuit voltage (OCV) up to 6 V *vs.* Li^+/Li°, and for the cathodic scan, from OCV down to -0.5 V *vs.* Li^+/Li°.

3. Results and Discussion

In the following we compare the physico-chemical properties of the neat ILs and the various IL based electrolytes containing either TFSI or FSI or both anions. The anions originate from both the Li-salt and the IL, why the balance between all components relative to one another can be altered. The focus is on revealing the role of each anion for basic properties; phase transitions, densities, viscosities, ionic conductivities, thermal stabilities, electrochemical stability windows, and charge carriers.

3.1 Phase transitions

In order for electrolyte performance to be predictable it is necessary to avoid phase transitions in the temperature range of interest. For a HT-LIB electrolyte this would comprise both the operation temperature, here approximately 100°C, and ambient or even lower temperatures during non-operation and shelf life. Furthermore, battery cycling can alter the phases present by introducing thermal variations and non-equilibrium situations in general. A first assessment of the promise of each electrolyte is made by detailed calorimetric studies. The phases and features present are highly dependent on the thermal history, as shown for pyrrolidinium and piperidinium based electrolytes by Furlani *et al.* [39], why all our electrolytes were measured the same way.

The melting (T_m) and glass transition temperatures (T_g) define the low temperature limit. Below the melting point the crystallinity severely restricts mobility and ion conduction; for totally or partially amorphous materials the same occurs below the glass transition temperature. The T_m and T_g for ILs and electrolytes are summarized in Table 1 and the DSC traces are shown in Figure 1. For the ILs, the T_g of EMITFSI is in excellent agreement with the literature [40, 41], while the T_m differ; Fredlake *et al.* [40] report a similar value, but Liu *et al.* a T_m *ca.* 8°C higher [41]. Deviations can arise from different measurement conditions and handling, *e.g.* amounts of sample or drying procedures, or different levels of purity. The T_m of EMIFSI is in excellent agreement with the literature [42]. The T_g of EMITFSI was obtained only at a fast cool rate, but no T_g was observed for EMIFSI. However, an exothermal peak at *ca.* -35°C, corresponding to a cold crystallization, indirectly supports the prior existence of a glassy state in EMIFSI.

The phase behaviour is strongly altered upon Li-salt addition, since much stronger ion-ion interactions are introduced [43, 44]. This leads to increased T_g and increased viscosity (see Figure 2), which worsen dynamics and transport properties [45, 46], but here the T_g increase only slightly: ≤ 12°C (maximum for $Li_{0.2}EMI_{0.8}TFSI$). Based on the results of all electrolytes, the effect of the anion can be elucidated; comparing the effects of adding LiFSI and LiTFSI the latter causes a larger increase in T_g. In the literature the interaction between TFSI and Li^+ has been calculated to be stronger than between FSI and Li^+ [43, 44], which results in a higher viscosity, hence a larger increase of T_g for samples with a larger amount of TFSI, resulting in the highest T_g of -79°C for the $Li_{0.2}EMI_{0.8}TFSI$ electrolyte. This is somewhat remarkable given the often-mentioned plasticizing effect of TFSI [10, 47], attributed to both its sheer size and internal flexibility [48, 49]. The equally flexible [50], but smaller FSI, may be just as plasticizing. The nature of the ion-ion interactions most likely plays an additional role.

Adding x=0.2 LiFSI or LiTFSI to EMIFSI result in *ca.* 20°C depressed melting points. Furthermore, all electrolytes remain liquid until *ca.* -22°C, in the best case until *ca.* -36°C, and the amount of crystalline phase basically decrease as a function of x. For $LiTFSI_{0.2}EMIFSI_{0.8}$ it is difficult to detect the melting peak (Figure 1). There is a subtle difference between the two ILs; the EMITFSI electrolytes (x=0.2) are fully amorphous, while a low temperature melting transition remains for the corresponding electrolytes with EMIFSI.

In summary, the eight electrolytes show wide liquid ranges, increasing with Li-salt concentration. The two electrolytes with the largest liquid ranges (EMITFSI and x=0.2) only exhibit a single glass transition. These results are consistent with the literature where Paillard *et al.* showed a widening of the liquid range with salt content and no crystalline phase at all for $Li_xPyr_{14(1-x)}FSI$ electrolytes with $x \geq 0.2$ [51]. A widening of the liquid range was also observed for mixtures of ILs containing FSI and TFSI [52, 53], but without a Li-salt. The presence of Li^+ is arguably of importance, since for our mixed electrolytes, the range was not additionally widened when both FSI and TFSI were present.

3.2 Density and Viscosity

The densities and viscosities are strongly dependent on the temperature and, in practice, important when the electrolyte first is to fill the porous separator. During battery operation, temperature differences can lead to mechanical stresses and worse electrode contact. The viscosity also has a strong impact on the rate of mass transport and on the wettability, affecting the rate of electrochemical reactions and general battery performance.

The densities and viscosities of the electrolytes increase with Li-salt concentration (Figure 2), suggesting an interaction between Li^+ and FSI and/or TFSI. The relative increase is larger for the TFSI based electrolytes. This was suggested to be arising from the stronger interactions of TFSI with Li^+ as compared to FSI as determined by *ab initio* calculations [43, 44]. Tsuzuki *et al.* further state that the in general higher viscosities of EMITFSI based samples are not only arising from the relatively larger TFSI, but also from stronger interactions between EMI and TFSI [43]. This is also in accordance with molecular dynamics (MD) simulations of EMIFSI and EMITFSI by Borodin *et al.* [54]

The viscosities of the electrolytes and the neat ILs were fitted by using a modified Vogel-Tammann-Fulcher (VTF) equation (eq. 2). All fits show a VTF behaviour. The VTF parameters of the best fits are summarized in Table 2.

$$\eta = \frac{\sqrt{T}}{\eta_0} exp\left(\frac{B}{T-T_0}\right) \qquad (2)$$

The density of EMIFSI (RT) is in agreement with the literature [55], while that of EMITFSI differs; Fredlake *et al.* [40] report a similar value, but Liu *et al.* [41] a slightly higher (by 2%, albeit using a different method) – just as for the comparison of T_m.

The viscosities decrease exponentially and the densities linearly with temperature – the former being only *ca.* 10-25% at 90°C compared to the values at 20°C. The measured viscosities for the neat ILs are in excellent agreement with the literature [43]. At 90°C the IL and electrolyte viscosities are close to that of the commercial organic solvent based electrolyte LP40 at 20°C (1M $LiPF_6$ in EC:DEC, 5.1 mPas), supporting IL based HT-LIB functionality. This is crucial, since conventional organic solvent and $LiPF_6$ based electrolytes are not stable above *ca.* 60°C [3]. Furthermore, at these elevated temperatures, the range of viscosities becomes quite narrow; 5.1 – 12.3 mPas, with the single largest viscosity decrease (>90%) observed for $Li_{0.2}EMI_{0.8}TFSI$ – and in general the relative decrease in viscosity at increased temperature, is a function also of Li-salt content (Figure 2). In summary, all electrolytes have appreciably low viscosities at 90°C, but FSI seems to promote somewhat lower electrolyte viscosities than TFSI, as previously reported in the literature [43, 56]. As for mixing the two anions, no distinct advantages are apparent here.

3.3 Ionic Conductivities

The ion transport within any electrolyte is influenced both by the viscosity and the type of charge carriers. In IL based electrolytes the situation can, however, be quite complicated as the matrix/solvent itself is composed of cations and anions, both contributing to the measure, and the latter solvating the Li^+ added as a Li-salt – a process which in general lowers the overall conductivity by creating larger complexes [21, 46]. In the here presented electrolytes, things are intrinsically even more complicated as competitive Li^+ coordination can occur between FSI and TFSI. The overall highest ionic conductivity was obtained for neat EMIFSI, *ca.* 3x that of EMITFSI, and in acceptable agreement with provider data and the literature [11, 41]. In general, the addition of Li-salt lowers the ionic conductivity, as a direct consequence of a higher viscosity due to the interaction between Li^+ and FSI and/or TFSI. The conductivities increase as a function of temperature and, at 80°C < T < 100°C, the conductivities are $\leq$ 6x those at RT and continues to increase to 150°C (end of data) for most of the electrolytes.

The anticipated decrease in ionic conductivity upon Li-salt addition is here confirmed for all but one group of electrolytes, $LiTFSI_xEMIFSI_{1-x}$, where the x=0.2 electrolyte, being one of the most conductive overall, is more conductive than x=0.1 for all temperatures. The $LiTFSI_{0.2}EMIFSI_{0.8}$ is also the only exception to another trend; for the same Li-salt content the conductivity increases with FSI content (Table 1). Overall, even the electrolyte with the lowest conductivity, $Li_{0.2}EMI_{0.8}TFSI$, has a conductivity high enough ($\geq 10^{-4}$ S cm^{-1}) to be considered for battery application [57], with the caveat that most of the conductivity likely being non-Li^+ related.

At low temperatures the abrupt increases in the conductivities of EMIFSI and EMITFSI (*ca.* -20°C, Figure 3) agree with the melting temperatures of the ILs (Table 1). At temperatures below the glass transition the ionic conductivities also increase non-monotonically for all systems, but with much less distinct features.

The conductivities were analysed in more detail by fitting the data between 90°C and close to T_g (or T_m) to a modified VTF equation (3) (Figure 3). The VTF parameters are summarized in Table 2. The Angell's strength parameter D ($B_\sigma = D*T_{0,\sigma}$) is often used to classify the fragility of liquids [58] and here all systems exhibit a D between 1.3 and 5.9, which reveals a fragile behaviour (D < 30), and hence a conductivity lower than expected for normal diffusion, due to cations and anions being coupled [59].

$$\sigma = \frac{A_\sigma}{\sqrt{T}} exp\left(\frac{-B_\sigma}{T-T_{0,\sigma}}\right) \qquad (3)$$

The basic data on density, viscosity, and conductivity is used to create a Walden plot for all the systems to further reveal differences in the ion association (Figure 4). The viscosity correlates to the ionic conductivity if the electrolytes follow the fractional Walden rule: [59]

$$\Lambda_m \eta^\gamma = C \qquad (4)$$

Here γ is a constant, $0 < \gamma \leq 1$, extractable from the slope of the Walden plot.

The usual reference, an aqueous solution of KCl with completely dissociated ions, γ = 1, is also added. All γ's are smaller than 1 and additionally the deviation increases with salt content. $LiTFSI_{0.2}EMIFSI_{0.8}$ is an exception with almost the same γ as $LiTFSI_{0.1}EMIFSI_{0.9}$ (see Table 2). Overall, the largest changes are observed for the $Li_xEMI_{(1-x)}FSI$ electrolytes, suggesting a stronger interaction between EMI and TFSI than with FSI and an increased ion association with Li^+. This agrees with both the viscosity and density data, literature data [43, 44, 56], and is consistent with the molecular level structure suggested by NMR spectroscopy [60], Raman spectroscopy coupled with DFT calculations, [33] and MD simulations [61, 62]. The data for the mixed electrolytes, however, propose an advantage of having both FSI and TFSI present at a certain ratio. The $LiTFSI_{0.2}EMIFSI_{0.8}$ electrolyte is among the most conductive electrolytes measured. A similar increase of the conductivity for a specific IL mixture was observed for $Pyr_{14}IM_{14x}TFSI_{(1-x)}$ at -20°C [53]. In accordance with previous IL and IL based electrolyte studies the investigated systems are classified as good ILs [59, 63].

3.4 Thermal stability

For HT-LIB application the electrolyte stability at high temperatures is critical. An increased temperature often leads to increased vapour pressures and/or decomposition – why monitoring the thermal stability of the electrolyte is extremely important to secure safe operation of a HT-LIB.

In the literature the EMIFSI and EMITFSI ILs decompose at approximately 225°C and 375°C, respectively [23]. LiFSI starts to decompose > 200°C [21], but the reaction rate becomes fast only from *ca.* 330°C. LiTFSI has the highest stability with a decomposition at *ca.* 380°C [64]. Thermal stability data on electrolytes using imidazolium based ILs with a Li-salt and both anions (xFSI) have not yet been reported.

From the TGA data EMIFSI decomposes at ~200°C and EMITFSI at ~300°C (Figure 5). The 25-75°C lower T_d compared to the literature [23] is due to different definitions for T_d (1 % vs. 5 % mass loss). Our results, at lower mass loss, are thus more conservative, emphasizing the need to keep the electrolytes safe. Moving to the electrolytes, the EMITFSI based are generally more stable than the EMIFSI based (Table 1), which again is most likely connected to the stronger interactions between EMI and TFSI. Adding LiFSI always lower the stability, but adding LiTFSI to EMIFSI increases the stability with respect to the neat IL. Overall, the T_d of the four mixed-anion electrolytes are within 30°C (199-229°C). Notably, the T_d of the EMITFSI electrolytes are almost unaffected by the presence of LiTFSI, while the addition of LiFSI lead to a *ca.* 100°C decrease in T_d with respect to the IL. Indeed, for the LiFSI salt there are two separable decompositions: at ~160°C and ~315°C. This is in stark contrast to the literature where also conflicting T_d are given: Han *et al.* reported a single T_d > 200°C and state a mass loss of only ~3 % from 200°C to 300°C [21], while Kubota *et al.* report a T_d of merely 70°C, during a long-term measurement [65]. No measurement details were given, such as information about the amount or ratio of the weight loss.

The decomposition of an IL based system can be slow, and thus the thermal stability as obtained by dynamic TGA exaggerated [51]. More precise determination of T_d are important for HT-LIB application and possible by applying isothermal TGA measurements [66, 67]; after 10 hours at 125°C we obtain a mass loss of *ca.* 10 % for $LiTFSI_{0.1}EMIFSI_{0.9}$ (Figure 5b) – a difference of *ca.* 85°C compared to the dynamic TGA results. The corresponding isothermal measurement on EMIFSI shows the difference to be not only quantitative, but also qualitative, since EMIFSI not decomposes, while in the dynamic TGA it has a worse stability as compared to $LiTFSI_{0.1}EMIFSI_{0.9}$. EMIFSI and EMITFSI were therefore mixed to create the same anion ratio as in $LiTFSI_{0.1}EMIFSI_{0.9}$, but without the presence of lithium, creating $EMI(TFSI_{0.1}FSI_{0.9})$, which proves to be stable in the isothermal TGA. Hence, an interaction between Li^+ and FSI or TFSI might trigger a decomposition of the least interacting species; the EMI cation.

In summary, all the IL based electrolytes seem to intrinsically exhibit thermal stabilities adequate for operation at 100°C, but care should be taken to always include data on stability using isothermal TGA [66], which might not only be lower as compared to data from dynamic TGA [12, 68], but also lead to qualitatively different conclusions. An additional complication in a real HT-LIB set-up is whether *e.g.* the electrode surfaces might trigger additional decomposition reactions [27, 69], but this is beyond the scope of this study.

3.5 Ionic interactions and local coordination

The basic physical properties and the ionic conductivity are needed to provide some credibility to functionality in a device, but for the latter it must be emphasized that for any IL based electrolytes the matrix contributes and thus decent ionic conductivities are always obtained. The crucial issue is, however, the useful ionic conductivity *i.e.* the one promoting Li^+ transport. As a further complication the charge carriers may change upon Li-salt addition by novel ion-ion interactions and coordination [33, 34, 62] – why molecular level detailed studies are crucial for any rational progress.

Raman spectroscopy is an especially suitable method due to the strong scattering cross-sections of the anions commonly used, *e.g.* TFSI and FSI, and since the lithium charge carrying complexes have been selectively identified in the literature [33, 70]. The ion-ion interactions within the neat ILs are weak [49], why in the analysis the EMI cation can be treated merely as a stand-by species (albeit sometimes causing band overlap).

For the anions, TFSI has been extensively studied by Raman spectroscopy, primarily the region of the intensive collective expansion and contraction mode [48, 71], which is centered at ~742 cm^{-1} and sensitive to both conformation and coordination changes [33, 48, 60, 72-74]. Two stable conformers of TFSI, cisoid (C_1) and transoid (C_2), were predicted early by *ab initio* calculations [47] and later quantified spectroscopically [48]. Both conformers co-exist in electrolytes at RT, due to the small conformational energy difference (2.2-3.5 kJ mol^{-1} [47, 48, 75]), and spectroscopically give rise to two closely spaced "free" anion bands at 738 and 741 cm^{-1} – observed as a single envelope [33, 48].

The addition of LiTFSI to TFSI based ILs introduces a new spectral feature at *ca.* 748 cm^{-1}, which is attributed to a $[Li(TFSI)_2]^-$ complex [33, 60] – identified also by NMR spectroscopy and further supported by MD simulations [60, 61]. This complex has a coordination number (CN) of 4, by virtue of doubly bidentate coordination, and hence a solvation number (SN) of 2. A SN=2 has emerged as quite a general feature [33], but the SN, and likely also the CN, has been shown to be a function of Li-salt concentration [34, 61]. There is also some controversy on the exact nature of the complexation, bidentate or not, based on conflicting results of MD simulations [76]. Méndez-Morales *et al.* have shown Li^+ to have a first solvation shell of strongly coordinated anions, a second shell of lithium ions, and a third of imidazolium cations [61].

The second anion, FSI, shows both similarities and differences compared to TFSI; it has two stable conformers, C_1 and C_2, with a calculated energy difference of 4.5 kJ mol^{-1} [77] and closely spaced Raman modes (calculated at 725 and 732 cm^{-1} [B3LYP/6-311+G(d)]$_{PCM}$). Experimentally, a single FSI envelope at *ca.* 731 cm^{-1} [70] (here at *ca.* 725 cm^{-1}) is in analogy with that observed for TFSI .

Fujii *et al.* reported a "free" FSI band at *ca.* 731 cm^{-1} and a coordination complex at *ca.* 744 cm^{-1} for an $Li_xEMI_{(1-x)}FSI$ electrolyte at room temperature [70]. They proposed the complex to be a doubly negatively charged $[Li(FSI)_3]^{2-}$ with CN=4 and SN=3, *i.e.* a combination of mono- and bi-dentate coordination. Such a doubly negatively charged species has also been proposed for NaTFSI in EMITFSI: $[Na(TFSI)_3]^{2-}$ [78]. For the $Li_xEMI_{(1-x)}FSI$ electrolyte at higher temperatures, *ca* 90°C, the SN decreased (with the CN unchanged), suggesting a change to a complex with two bidentately coordinated FSI [70, 77].

Solano *et al.* predicted the coordination of Li^+ in an Li-FSI IL-based electrolyte (CN=3.9) to be more extensive than in the corresponding Li-TFSI electrolyte (CN=3.4), by MD simulations [76]. This was interpreted as due to the anion size difference and/or steric effects, and it was suggested that Li^+ is coordinated to 4 oxygen atoms from 4 unique FSI, $[Li(FSI)_4]^{3-}$. They further proposed the CN for Li-TFSI to result from a solvation of Li^+ by 3 TFSI.

With all the above basics of ion-ion interactions and coordination for the TFSI and FSI anions in IL matrices at hand, we now turn to the detailed analysis of our electrolytes – starting with those

comprising only a single anion before treating the more complicated cases.

The $Li_xEMI_{(1-x)}TFSI$ electrolytes

Starting with EMITFSI, the envelope centered at ~742 cm^{-1} is according to the literature due to two overlapping bands originating from the two conformers of the "free" TFSI anion [48]. In addition, we found adding a minor feature at *ca.* 745 cm^{-1}, likely due to EMI (which also has two spectrally closely spaced conformers in this region [72]), to improve the fit considerably (Figure 6). Addition of LiTFSI leads to a new band at 747 cm^{-1}, in agreement with the literature assigned to the $[Li(TFSI)_2]^-$ complex [33].

Deconvolution and application of eq. 1 result in an estimate of SN as a function of temperature (Figure 7). The SN decrease slightly with temperature (1.8-1.5), but is overall close to 2, which is somewhat lower (*ca.* 0.3 at 30°C and 0.1 at 120°C) than previously reported [33, 79] and mainly due to our account of the EMI band in the deconvolution. Thus, most of the Li^+ in these electrolytes are transported as part of negatively charged $[Li(TFSI)_2]^-$ species – which may seem awkward, but still enables functional LIBs [11].

The $Li_xEMI_{(1-x)}FSI$ electrolytes

The spectrum of EMIFSI shows two main features at 702 cm^{-1} and 725 cm^{-1} (Figure 8). For the deconvolution of the electrolyte spectra we apply the same EMI band as we did for the TFSI based electrolytes (744 cm^{-1}) and account for both FSI conformers (at *ca.* 725 and 731 cm^{-1}). We note in passing that the width of the two FSI bands (FWHM≈10-20) are larger than those for TFSI (≈7) [33], which could reveal higher dynamic disorder. The SNs obtained (Figure 7); 2.4 (x=0.1) and 2.1 (x=0.2), differ from the SN of 3 predicted by Fujii *et al.* [70], but are clearly larger than for the TFSI system; 1.8 (x=0.1) and 1.9 (x=0.2). These results agree with the trend from the MD simulations of Solano *et al.* albeit having much larger SNs [76].

Electrolytes containing both TFSI and FSI

In a Raman study by Huang *et al.* LiFSI and LiTFSI were added to $Pyr_{13}FSI$, to obtain electrolytes with mixed anions [80], and concluded Li^+ to be preferentially coordinated by FSI. However, a recent NMR study of Lesch *et al.* proposed TFSI to be the preferred ligand of Li^+ and forming aggregates referred to as lithium dimers (Li-TFSI-Li) in both $LiTFSI_xEMIFSI_{1-x}$ and $LiFSI_xEMITFSI_{1-x}$ electrolytes [81]. These latter results agree with the computed stronger interactions predicted for Li-TFSI, as compared to Li-FSI [43, 44]. Yet, the overall picture is thus ambiguous.

The analysis we have made above on the nature of the charge carriers, when there is only a single anion present, is far from simple, but it benefits from a limited set of possibilities. When we use LiFSI in EMITFSI or LiTFSI in EMIFSI we expand the set of possibilities dramatically. At first sight there are three types of coordination possible: by FSI or TFSI, or a combination of both. If there is an anion preference, it should be able to elucidate this. In more detail, however, the Raman spectra will be products of bands due to many possible components; the "free" anions, both present in two conformers, totally four bands, and various complexes either of the pure or mixed types and for the latter we know neither SN nor CN. If we also account for the conformations of FSI and TFSI within the various complexes it is clear that the task of proper deconvolution becomes extremely challenging.

Qualitatively, however, it is possible to differentiate some plausible coordination scenarios. In the two $LiFSI_xEMITFSI_{(1-x)}$ electrolytes, for example, there is an excess of TFSI and only a 1:1 ratio of Li:FSI, and thus a strong preferential coordination of FSI to Li^+ would result in the absence of the bands due to "free" FSI. Experimentally, however, we do find this band to be present.

For the $LiTFSI_xEMIFSI_{(1-x)}$ electrolytes the situation is different. Ideally there would be no, or only minor, signs of "free" TFSI, since there is an abundance of FSI, but there is a 1:1 ratio of Li:TFSI and a preference for TFSI. Indeed, in Figure 9b the band at 747 cm^{-1} assigned to the $[Li(TFSI)_2]^-$ complex is clearly present, but there is also a feature at ca 742 cm^{-1}. The latter could be assigned as "free" TFSI (742 cm^{-1}), but also to the $[Li(FSI)_3]^{2-}$ complex (743 cm^{-1}). Both assignments rely on FSI taking part in the coordination of Li^+, which is likely due to the much higher concentration of FSI, but it is not an unambiguous sign of "free" TFSI.

The manifold problems of: i) overlapping "free" and coordinated anions of various kinds and ii) the possibility for new various complexes of unknown SN and CN are a challenge. Unknown frequencies, Raman scattering cross-sections, and band-widths, makes a quantitative analysis difficult. Yet, the effect of increasing the lithium salt concentration shows an increased interaction between Li^+ and FSI or TFSI, but the detailed coordination of Li^+ to the anions is again, fundamentally, not possible to elucidate.

In summary, for the electrolytes with TFSI or FSI as the exclusive anions, we find that Li^+ is solvated by approximately two TFSI, while the SN of Li^+ with FSI is slightly higher (SN=2.1-2.4) depending on the salt concentration. The higher SNs for FSI agree qualitatively with MD results, [76] albeit the SN of the latter are predicted to be much larger.

The detailed solvation of Li^+ in the mixed anion electrolytes is not clearly resolved, as Raman data does not exclude the presence of either anion in the solvation shell of Li^+ in any of the four mixed anion electrolytes. The structures predicted from *ab initio* and DFT calculations, [43, 44] as well as from NMR results, [81] suggest a predominant coordination of Li^+ by TFSI. Our present results show a more complex picture.

3.6 Electrochemical stability window

Adequate electrochemical stability of the electrolytes is crucial for their usage in LIB. Wide ESW *i.e.* an anodic and cathodic limit ≥ 5 V and ≤ 0 V *vs.* Li^+/Li°, is beneficial as it at least in principle, provides a wide selection of electrode materials possible.

The voltammograms resulting from the LSV measurements are shown in Figure 10 and with respect to the anodic stability, the electrolytes with FSI as the exclusive anion start to decompose at close to 4 V *vs.* Li^+/Li°. The electrolytes with TFSI as the exclusive anion are more stable (≥ 5 V *vs.* Li^+/Li°). The mixed anion electrolytes all have anodic stabilities between 4.5 and 5 V *vs.* Li^+/Li°. Increased anodic stability with TFSI content is a clear trend. For the cathodic stability, all electrolytes are stable to potentials *ca.* -0.1 V *vs.* Li^+/Li°, but with various resulting currents – much larger in the case of FSI being the sole or dominant anion. These

observations may also be coupled to lithium plating rather than any electrochemical decomposition [82].

4. Conclusions

The aim of this study was to investigate the fundamental properties of electrolytes for their possible application in high temperature, *ca.* 100°C, LIBs. Overall, the properties (densities, viscosities, *etc.*) of all systems investigated are strikingly similar, but both the amount of Li salt and the balance of FSI/TFSI affect their practical promise as battery electrolytes. The $LiTFSI_{0.2}EMIFSI_{0.8}$ electrolyte is especially promising, due to its high thermal stability in the working range and its high ionic conductivity. This might arise from a specific solvation of Li^+ by TFSI and FSI, at a given Li-salt concentration, which seems to result in a synergetic advantage. The detailed Raman analysis leads to SNs of *ca.* 2 for all the analysed electrolytes, somewhat higher for the FSI based and lowered at higher temperatures for the TFSI based. These observations are corroborated by literature DFT, MD, and NMR results. The Raman analysis of the mixed anion electrolytes is inherently laden with ambiguities why no distinct anion coordination preference can be concluded, which infers the possibility of a TFSI/FSI mixed solvation and also various charge carriers possible. The physico-chemical properties, *e.g.* the exception in the trend of ionic conductivities for one of the mixed electrolytes, point towards possible general synergetic effects for mixed anion IL based electrolytes. Finally, we stress that in terms of viscosity, and hence ion transport at large, these IL based electrolytes are on par with organic based electrolytes when taking into account their foreseen operating temperatures.

Acknowledgements

The authors gratefully acknowledge the financial support, for the project "Kraftfulla batterier med svenska material" provided by the Swedish Foundation for Strategic Research (SSF).

Notes and references

1. M. Armand and J. M. Tarascon, *Nature*, 2008, **451**, 652-657.
2. J. B. Goodenough and K.-S. Park, *J. Am. Chem. Soc.*, 2013, **135**, 1167-1176.
3. S. Wilken, P. Johansson and P. Jacobsson, *Solid State Ionics*, 2012, **225**, 608-610.
4. S. Aparicio, M. Atilhan and F. Karadas, *Ind. Eng. Chem. Res.*, 2010, **49**, 9580-9595.
5. M. Armand, F. Endres, D. R. MacFarlane, H. Ohno and B. Scrosati, *Nat. Mater.*, 2009, **8**, 621-629.
6. A. Matic and B. Scrosati, *MRS Bulletin*, 2013, **38**, 533-537.
7. J. Pitawala, A. Matic, A. Martinelli, P. Jacobsson, V. Koch and F. Croce, *J. Phys. Chem. C*, 2009, **113**, 10607-10610.
8. J. D. Holbrey and K. R. Seddon, *Clean Technologies and Environmental Policy*, 1999, **1**, 223-236.
9. F. Endres and S. Zein El Abedin, *Phys. Chem. Chem. Phys.*, 2006, **8**, 2101-2116.
10. A. Fernicola, B. Scrosati and H. Ohno, *Ionics*, 2006, **12**, 95-102.
11. B. Garcia, S. Lavallée, G. Perron, C. Michot and M. Armand, *Electrochim. Acta*, 2004, **49**, 4583-4588.
12. Q. Zhou, W. A. Henderson, G. B. Appetecchi, M. Montanino and S. Passerini, *J. Phys. Chem. B*, 2008, **112**, 13577-13580.
13. H. Sakaebe, H. Matsumoto and K. Tatsumi, *J. Power Sources*, 2005, **146**, 693-697.
14. S. Seki, Y. Kobayashi, H. Miyashiro, Y. Ohno, Y. Mita, N. Terada, P. Charest, A. Guerfi and K. Zaghib, *J. Phys. Chem. C*, 2008, **112**, 16708-16713.
15. M. A. Navarra, *MRS Bulletin*, 2013, **38**, 548-553.
16. P. M. Bayley, G. H. Lane, D. R. MacFarlane and M. Forsyth, *Phys. Chem. Chem. Phys.*, 2009, **11**, 7202-7208.
17. G. H. Lane, A. S. Best, D. R. MacFarlane, M. Forsyth, P. M. Bayley and A. F. Hollenkamp, *Electrochim. Acta*, 2010, **55**, 8947-8952.
18. C. Arbizzani, G. Gabrielli and M. Mastragostino, *J. Power Sources*, 2011, **196**, 4801-4805.
19. M. Nádherná, J. Reiter, J. Moškon and R. Dominko, *J. Power Sources*, 2011, **196**, 7700-7706.
20. Y. Matsui, M. Yamagata, S. Murakami, Y. Saito, T. Higashizaki, E. Ishiko, M. Kono and M. Ishikawa, *J. Power Sources*, 2015, **279**, 766-773.
21. H.-B. Han, S.-S. Zhou, D.-J. Zhang, S.-W. Feng, L.-F. Li, K. Liu, W.-F. Feng, J. Nie, H. Li and X.-J. Huang, *J. Power Sources*, 2011, **196**, 3623-3632.
22. E. Jónsson, S. Wilken and P. Johansson, *In manuscript*, 2015.
23. M. Ishikawa, T. Sugimoto, M. Kikuta, E. Ishiko and M. Kono, *J. Power Sources*, 2006, **162**, 658-662.
24. A. Lahiri, T. J. Schubert, B. Iliev and F. Endres, *Phys. Chem. Chem. Phys.*, 2015, **17**, 11161-11164.
25. M. Yamagata, Y. Matsui, T. Sugimoto, M. Kikuta, T. Higashizaki, M. Kono and M. Ishikawa, *J. Power Sources*, 2013, **227**, 60-64.
26. M. Yamagata, N. Nishigaki, S. Nishishita, Y. Matsui, T. Sugimoto, M. Kikuta, T. Higashizaki, M. Kono and M. Ishikawa, *Electrochim. Acta*, 2013, **110**, 181-190.
27. R. Costa, C. M. Pereira and A. F. Silva, *Electrochim. Acta*, 2015, **167**, 421-428.
28. T. Sugimoto, M. Kikuta, E. Ishiko, M. Kono and M. Ishikawa, *J. Power Sources*, 2008, **183**, 436-440.
29. H. Matsumoto and K. Kubota, *ECS Transactions*, 2014, **64**, 425-432.
30. L. Bodenes, R. Naturel, H. Martinez, R. Dedryvère, M. Menetrier, L. Croguennec, J.-P. Pérès, C. Tessier and F. Fischer, *J. Power Sources*, 2013, **236**, 265-275.
31. J. Mun, Y. S. Jung, T. Yim, H. Y. Lee, H.-J. Kim, Y. G. Kim and S. M. Oh, *J. Power Sources*, 2009, **194**, 1068-1074.
32. M. J. Marczewski, B. Stanje, I. Hanzu, M. Wilkening and P. Johansson, *Phys. Chem. Chem. Phys.*, 2014, **16**, 12341-12349.
33. J.-C. Lassègues, J. Grondin, C. Aupetit and P. Johansson, *J. Phys. Chem. A*, 2009, **113**, 305-314.
34. J. Pitawala, A. Martinelli, P. Johansson, P. Jacobsson and A. Matic, *J. Non-Cryst. Solids*, 2015, **407**, 318-323.
35. V. Barone and M. Cossi, *J. Phys. Chem. A*, 1998, **102**, 1995-2001.
36. J. Scheers, E. Jónsson, P. Jacobsson and P. Johansson, *J. Electrochem. Soc.*, 2012, **80**, 18-25.

37. J. Scheers, L. Niedzicki, G. Z. Zukowska, P. Johansson, W. Wieczorek and P. Jacobsson, *Phys. Chem. Chem. Phys.*, 2011, **13**, 11136-11147.
38. M. J. Frisch, G. W. Trucks, H. B. Schlegel, G. E. Scuseria, M. A. Robb, J. R. Cheeseman, G. Scalmani, V. Barone, B. Mennucci, G. A. Petersson, H. Nakatsuji, M. Caricato, X. Li, H. P. Hratchian, A. F. Izmaylov, J. Bloino, G. Zheng, J. L. Sonnenberg, M. Hada, M. Ehara, K. Toyota, R. Fukuda, J. Hasegawa, M. Ishida, T. Nakajima, Y. Honda, O. Kitao, H. Nakai, T. Vreven, J. A. Montgomery Jr., J. E. Peralta, F. Ogliaro, M. J. Bearpark, J. Heyd, E. N. Brothers, K. N. Kudin, V. N. Staroverov, R. Kobayashi, J. Normand, K. Raghavachari, A. P. Rendell, J. C. Burant, S. S. Iyengar, J. Tomasi, M. Cossi, N. Rega, N. J. Millam, M. Klene, J. E. Knox, J. B. Cross, V. Bakken, C. Adamo, J. Jaramillo, R. Gomperts, R. E. Stratmann, O. Yazyev, A. J. Austin, R. Cammi, C. Pomelli, J. W. Ochterski, R. L. Martin, K. Morokuma, V. G. Zakrzewski, G. A. Voth, P. Salvador, J. J. Dannenberg, S. Dapprich, A. D. Daniels, Ö. Farkas, J. B. Foresman, J. V. Ortiz, J. Cioslowski and D. J. Fox, Gaussian, Inc., Wallingford, CT, USA, 2009.
39. M. Furlani, I. Albinsson, B. E. Mellander, G. B. Appetecchi and S. Passerini, *Electrochim. Acta*, 2011, **57**, 220-227.
40. C. P. Fredlake, J. M. Crosthwaite, D. G. Hert, S. N. V. K. Aki and J. F. Brennecke, *Chem. Eng. Data*, 2004, **49**, 954-964.
41. K. Liu, Y.-X. Zhou, H.-B. Han, S.-S. Zhou, W.-F. Feng, J. Nie, H. Li, X.-J. Huang, M. Armand and Z.-B. Zhou, *Electrochim. Acta*, 2010, **55**, 7145-7151.
42. T. Umecky, Y. Saito, S. Tsuzuki and H. Matsumoto, *ECS Transactions*, 2009, **16**, 39-51.
43. S. Tsuzuki, K. Hayamizu and S. Seki, *J. Phys. Chem. B*, 2010, **114**, 16329-16336.
44. P. Johansson, *Phys. Chem. Chem. Phys.*, 2007, **9**, 1493-1498.
45. J. Pitawala, J.-K. Kim, P. Jacobsson, V. Koch, F. Croce and A. Matic, *Disc. Faraday Soc.*, 2012, **154**, 71-71.
46. A. Martinelli, A. Matic, P. Jacobsson, L. Börjesson, A. Fernicola and B. Scrosati, *J. Phys. Chem. B*, 2009, **113**, 11247-11251.
47. P. Johansson, S. P. Gejji, J. Tegenfeldt and J. Lindgren, *Electrochim. Acta*, 1998, **43**, 1375-1379.
48. M. Herstedt, M. Smirnov, P. Johansson, M. Chami, J. Grondin, L. Servant and J.-C. Lassègues, *J. Raman Spectrosc.*, 2005, **36**, 762-770.
49. K. Angenendt and P. Johansson, *J. Phys. Chem. B*, 2011, **115**, 7808-7813.
50. J. N. Canongia Lopes, K. Shimizu, A. A. H. Pádua, Y. Umebayashi, S. Fukuda, K. Fujii and S.-i. Ishiguro, *J. Phys. Chem. B*, 2008, **112**, 9449-9455.
51. E. Paillard, Q. Zhou, W. A. Henderson, G. B. Appetecchi, M. Montanino and S. Passerini, *J. Electrochem. Soc.*, 2009, **156**, A891-A895.
52. M. Kunze, S. Jeong, E. Paillard, M. Winter and S. Passerini, *J. Phys. Chem. C*, 2010, **114**, 12364-12369.
53. M. Montanino, M. Moreno, F. Alessandrini, G. B. Appetecchi, S. Passerini, Q. Zhou and W. A. Henderson, *Electrochim. Acta*, 2012, **60**, 163-169.
54. O. Borodin, W. Gorecki, G. D. Smith and M. Armand, *J. Phys. Chem. B*, 2010, **114**, 6786-6798.
55. T. Umecky, Y. Saito, Y. Okumura, S. Maeda and T. Sakai, *J. Phys. Chem. B*, 2008, **112**, 3357-3364.
56. H. Matsumoto, H. Sakaebe, K. Tatsumi, M. Kikuta, E. Ishiko and M. Kono, *J. Power Sources*, 2006, **160**, 1308-1313.
57. J. B. Goodenough and Y. Kim, *Chem. Mater.*, 2010, **22**, 587-603.
58. C. A. Angell, *J. Non-Cryst. Solids*, 1991, **131-133**, 13-31.
59. C. A. Angell, Y. Ansari and Z. Zhao, *Disc. Faraday Soc.*, 2012, **154**, 9-27.
60. S. Duluard, J. Grondin, J.-L. Bruneel, I. Pianet, A. Grélard, G. Campet, M.-H. Delville and J.-C. Lassègues, *J. Raman Spectrosc.*, 2008, 627-632.
61. T. Mendez-Morales, J. Carrete, S. Bouzon-Capelo, M. Perez-Rodriguez, O. Cabeza, L. J. Gallego and L. M. Varela, *J Phys Chem B*, 2013, **117**, 3207-3220.
62. M. J. Monteiro, F. F. C. Bazito, L. J. A. Siqueira, M. C. C. Ribeiro and R. M. Torresi, *J. Phys. Chem. B*, 2008, **112**, 2102-2109.
63. K. Ueno, H. Tokuda and M. Watanabe, *Phys. Chem. Chem. Phys.*, 2010, **12**, 1649-1658.
64. A. B. McEwen, H. L. Ngo, K. Lecompte and J. L. Goldman, *J. Electrochem. Soc.*, 1999, **146**, 1687-1695.
65. K. Kubota, T. Nohira, T. Goto and R. Hagiwara, *Electrochem. Comm.*, 2008, **10**, 1886-1888.
66. Y. Cao and T. Mu, *Ind. Eng. Chem. Res.*, 2014, **53**, 8651-8664.
67. T. J. Wooster, K. M. Johanson, K. J. Fraser, D. R. MacFarlane and J. L. Scott, *Green Chem.*, 2006, **8**, 691.
68. J. Salgado, J. J. Parajó, J. Fernández and M. Villanueva, *J. Chem. Thermodyn.*, 2014, **74**, 51-57.
69. D. Bedrov, J. Vatamanu and Z. Hu, *J. Non-Cryst. Solids*, 2015, **407**, 339-348.
70. K. Fujii, H. Hamano, H. Doi, X. Song, S. Tsuzuki, K. Hayamizu, S. Seki, Y. Kameda, K. Dokko, M. Watanabe and Y. Umebayashi, *J. Phys. Chem. C*, 2013, **117**, 19314-19324.
71. L. J. Hardwick, M. Holzapfel, A. Wokaun and P. Novák, *J. Raman Spectrosc.*, 2007, **38**, 110-112.
72. J.-C. Lassègues, J. Grondin, R. Holomb and P. Johansson, *J. Raman Spectrosc.*, 2007, **38**, 551-558.
73. Y. Umebayashi, S. Mori, K. Fujii, S. Tsuzuki, S. Seki, K. Hayamizu and S.-i. Ishiguro, *J. Phys. Chem. B*, 2010, **114**, 6513-6521.
74. A. Martinelli, A. Matic, P. Johansson, P. Jacobsson, L. Börjesson, A. Fernicola, S. Panero, B. Scrosati and H. Ohno, *J. Raman Spectrosc.*, 2011, **42**, 522-528.
75. J. N. C. Lopes, K. Shimizu, A. A. H. Pádua, Y. Umebayashi, S. Fukuda, K. Fujii and S.-i. Ishiguro, *J. Phys. Chem. B*, 2008, **112**, 1465-1472.
76. C. J. F. Solano, S. Jeremias, E. Paillard, D. Beljonne and R. Lazzaroni, *J. Chem. Phys.*, 2013, **139**, 034502.
77. K. Fujii, S. Seki, S. Fukuda, R. Kanzaki, T. Takamuku, Y. Umebayashi and S.-i. Ishiguro, *J. Phys. Chem. B*, 2007, **111**, 12829-12833.
78. D. Monti, E. Jónsson, M. R. Palacín and P. Johansson, *J. Power Sources*, 2014, **245**, 630-636.
79. J.-C. Lassègues, J. Grondin and D. Talaga, *Phys. Chem. Chem. Phys.*, 2006, **8**, 5629-5632.
80. J. Huang and A. F. Hollenkamp, *J. Phys. Chem. C*, 2010, **114**, 21840-21847.
81. V. Lesch, S. Jeremias, A. Moretti, S. Passerini, A. Heuer and O. Borodin, *J. Phys. Chem. B*, 2014, **118**.
82. R.-S. Kühnel, N. Böckenfeld, S. Passerini, M. Winter and A. Balducci, *Electrochim. Acta*, 2011, **56**, 4092-4099.

PCCP

ARTICLE

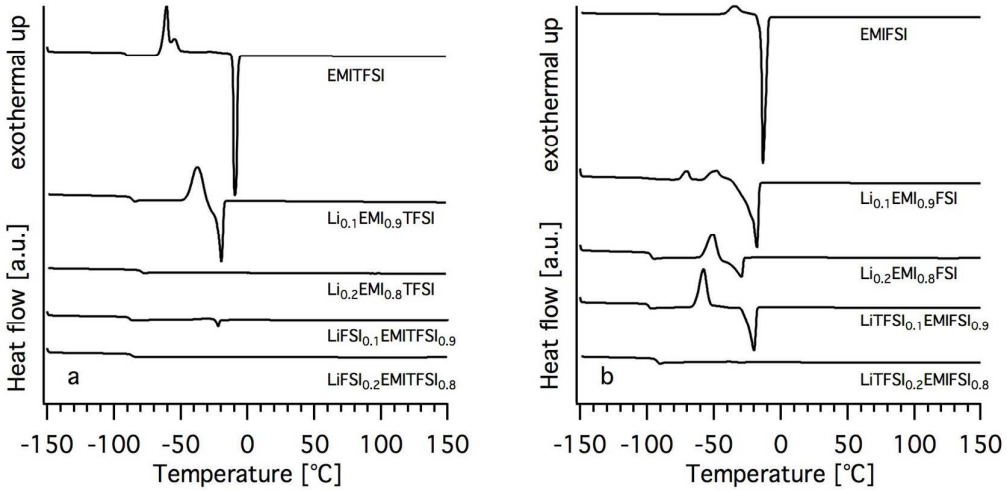

Figure 1: DSC heating traces of a) EMITFSI and the corresponding electrolytes with LiTFSI or LiFSI, and b) EMIFSI and the corresponding electrolytes.

Table 1: Glass transitions, melting temperatures, ionic and molar conductivities (20°C and 90°C), and decomposition temperatures for ILs and electrolytes.

Material	T_g [°C]	T_m [°C]	$\sigma_{20°C}$ [mS cm^{-1}]	$\sigma_{90°C}$ [mS cm^{-1}]	$\Lambda_{m\ 20°C}$ [S cm^2 mol^{-1}]	$\Lambda_{m\ 90°C}$ [S cm^2 mol^{-1}]	T_d [°C]
EMIFSI	-	-16	15.3	60.0	3.08	12.6	201
$Li_{0.1}EMI_{0.9}FSI$	-99	-29	6.6	27.0	1.27	5.43	178
$Li_{0.2}EMI_{0.8}FSI$	-97	-36	3.7	13.3	0.61	2.31	161
$LiTFSI_{0.1}EMIFSI_{0.9}$	-99	-28	4.6	17.1	0.90	3.50	211
$LiTFSI_{0.2}EMIFSI_{0.8}$	-92	-34	5.0	21.4	0.94	4.27	229
EMITFSI	-91	-18	5.3	23.5	1.38	6.39	302
$Li_{0.1}EMI_{0.9}TFSI$	-86	-22	2.8	12.9	0.68	3.32	288
$Li_{0.2}EMI_{0.8}TFSI$	-79	-	1.7	9.4	0.39	2.32	303
$LiFSI_{0.1}EMITFSI_{0.9}$	-88	-24	3.7	17.4	0.90	4.41	213
$LiFSI_{0.2}EMITFSI_{0.8}$	-87	-	2.6	13.2	0.58	3.14	199
LiFSI							160 315
LiTFSI							333

Table 2: VTF-parameters for the fits of the viscosities and conductivities.

Material	A_η [$mPa^{-1}\ s^{-1}\ K^{-1/2}$]	B_η [K]	$T_{0,\eta}$ [K]	R_η^2	A_σ [$mS\ K^{1/2}\ cm^{-1}$]	B_σ [K]	D_σ	$T_{0,\sigma}$ [K]	R_σ^2	γ
EMIFSI	138	836	141	0.999	33939	780	5.86	133	0.923	0.969
$Li_{0.1}EMI_{0.9}FSI$	121	819	133	0.998	8107	545	3.30	165	0.940	0.935
$Li_{0.2}EMI_{0.8}FSI$	111	819	127	0.996	2308	396	2.16	183	0.925	0.787
$LiTFSI_{0.1}EMIFSI_{0.9}$	117	800	129	0.996	3675	462	2.68	172	0.986	0.844
$LiTFSI_{0.2}EMIFSI_{0.8}$	104	794	120	0.990	6012	512	2.96	173	0.987	0.845
EMITFSI	125	803	122	0.997	7466	546	3.23	169	0.985	0.870
$Li_{0.1}EMI_{0.9}TFSI$	122	820	114	0.999	2701	412	2.15	191	0.997	0.791
$Li_{0.2}EMI_{0.8}TFSI$	114	837	105	0.995	2904	485	2.58	188	0.976	0.774
$LiFSI_{0.1}EMITFSI_{0.9}$	115	796	115	0.986	4276	457	2.48	184	0.985	0.840
$LiFSI_{0.2}EMITFSI_{0.8}$	90	760	102	0.973	3066	424	2.20	193	0.987	0.785

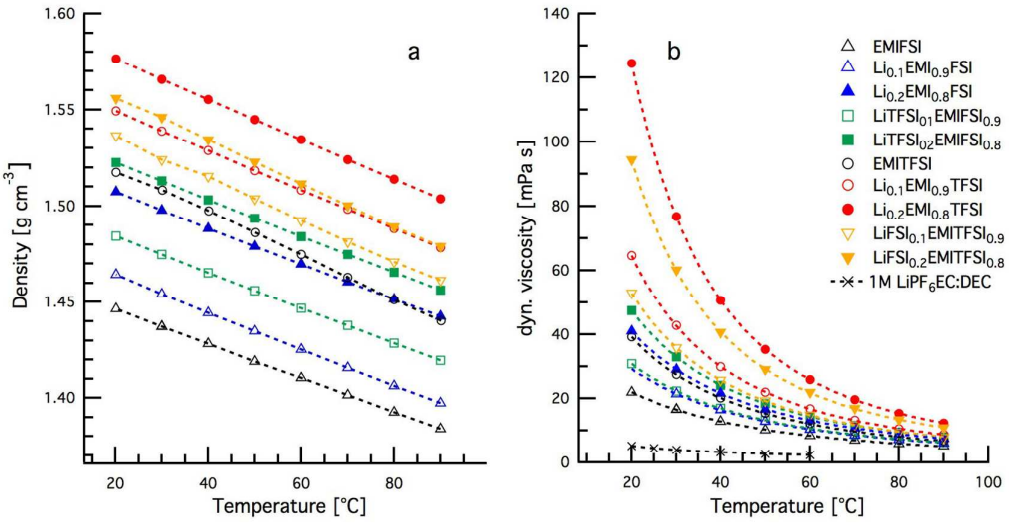

Figure 2: Densities (a) and viscosities (b) as functions of temperature. Data for an organic solvent based electrolyte LP40 (1M $LiPF_6$:EC:DEC) is added in (b). The viscosity curves (b) are the respective VTF-fits.

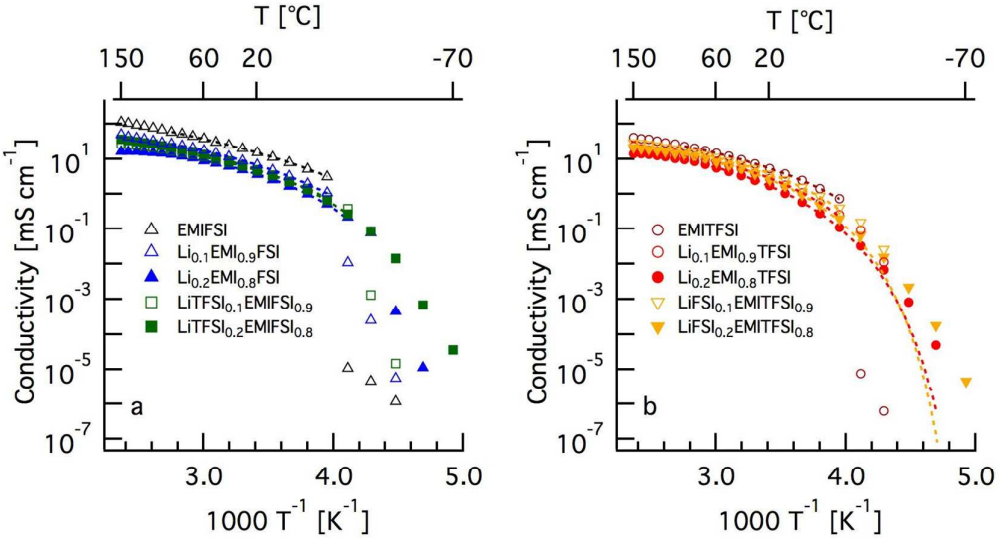

Figure 3: Ionic conductivities of EMIFSI (a) and EMITFSI (b) based electrolytes from 150°C to -80°C. The dotted lines are VTF-fits (T_g or T_m < T < 90°C).

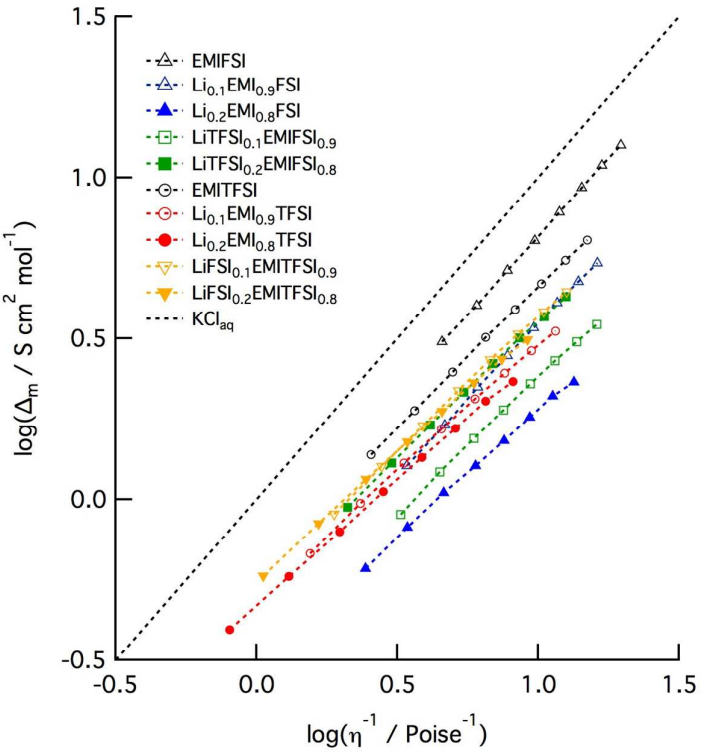

Figure 4: Walden plot for the neat ILs and the electrolytes using data between 20°C and 90°C.

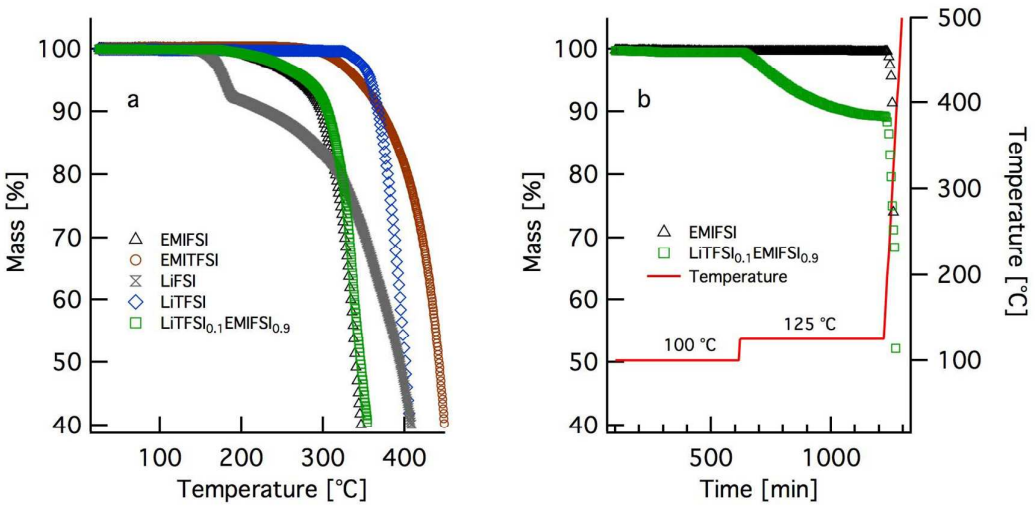

Figure 5: Dynamic TGA results of the neat ILs and Li-salts (a) and isothermal TGA results of EMIFSI and $LiTFSI_{0.1}EMIFSI_{0.9}$ (b).

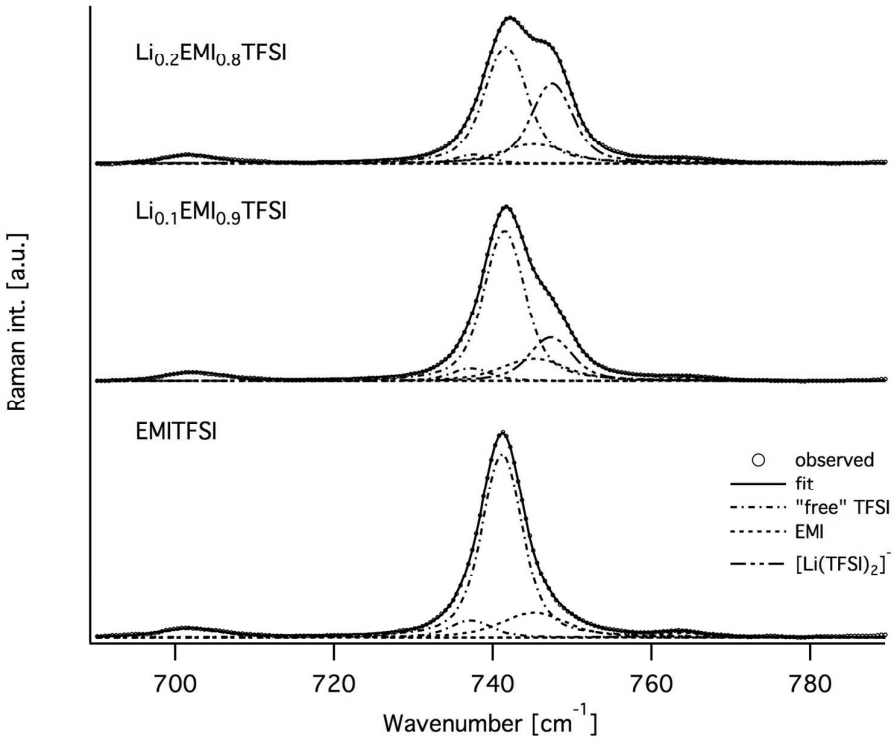

Figure 6: Deconvoluted Raman spectra of $Li_xEMI_{1-x}TFSI$

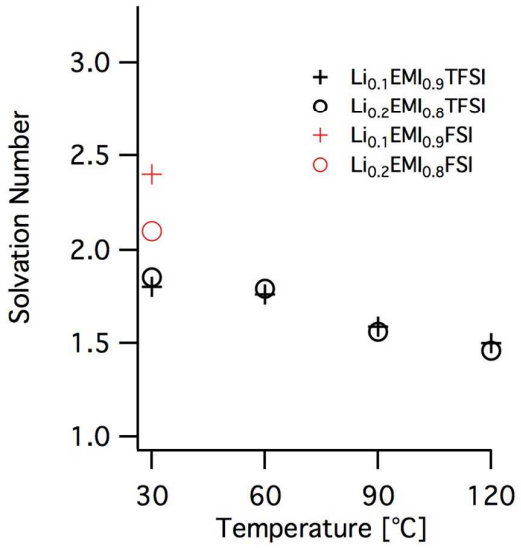

Figure 7: The SN of Li^+ for $Li_xEMI_{(1-x)}TFSI$ (x=0.1 and 0.2) as a function of temperature and for $Li_xEMI_{(1-x)}FSI$ at 30°C (x=0.1 and 0.2).

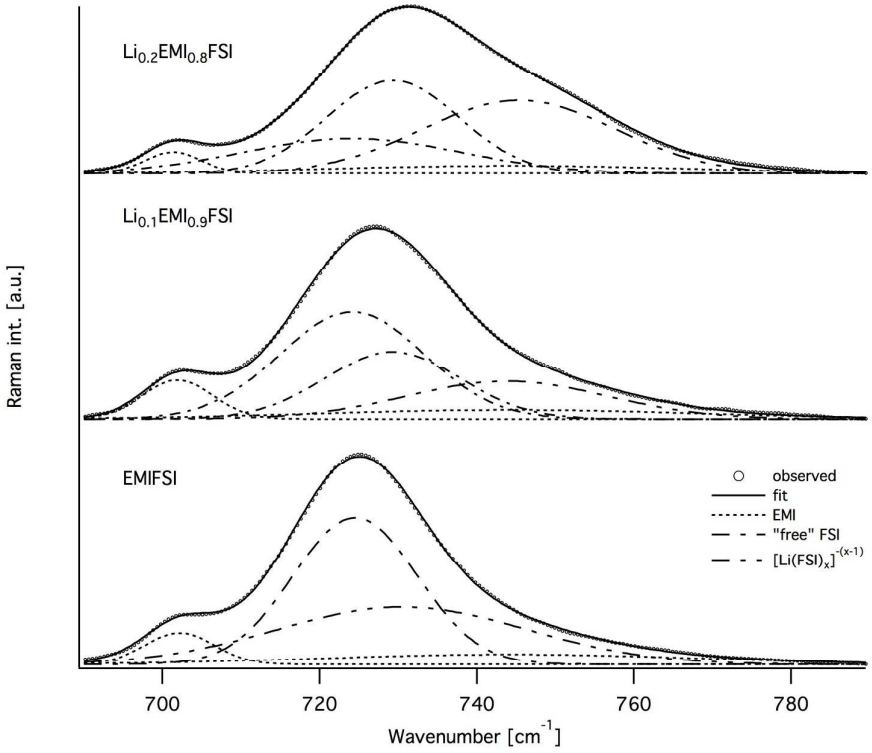

Figure 8: Deconvoluted Raman spectra of $Li_xEMI_{1-x}FSI$.

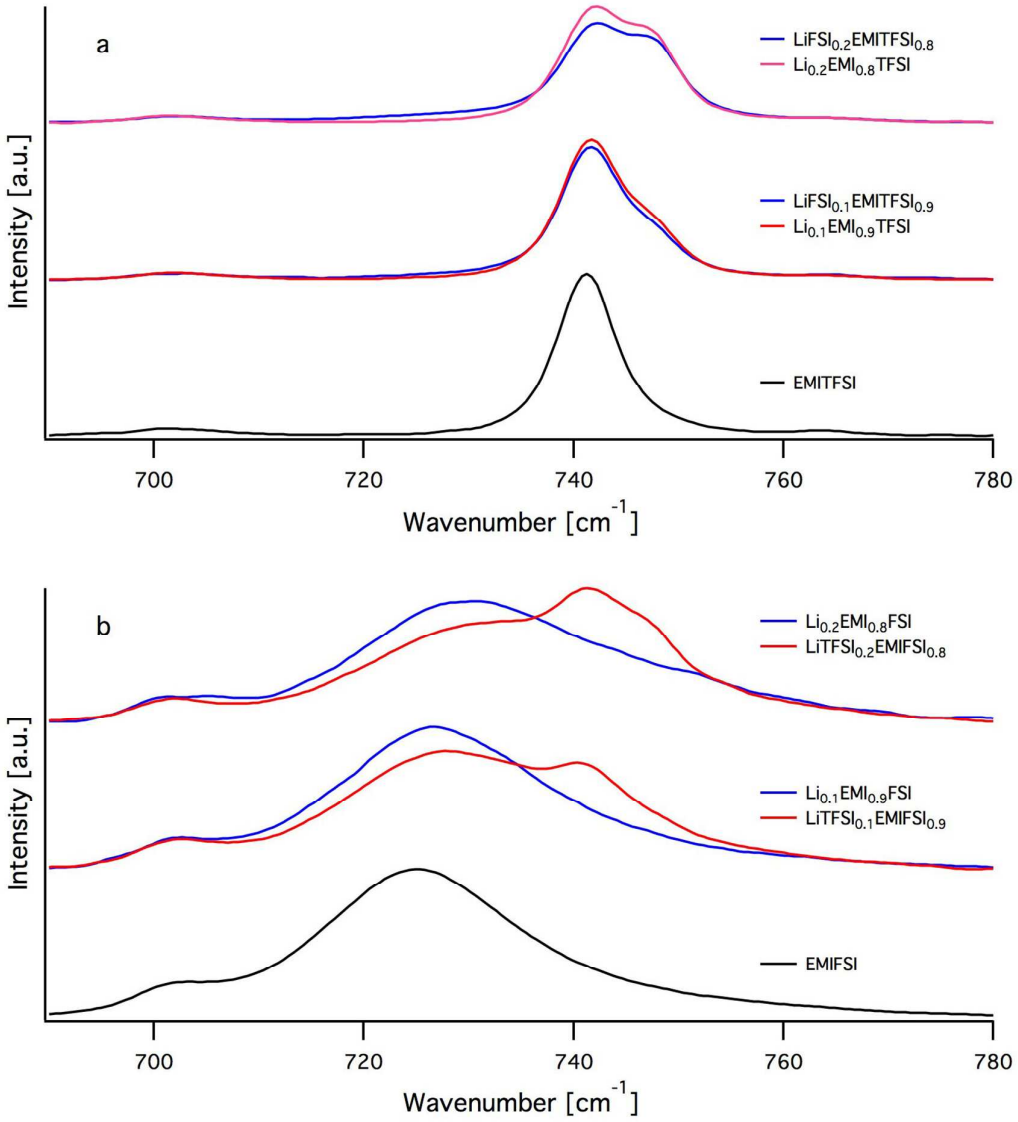

Figure 9: The influence of LiFSI and LiTFSI on the Raman spectra of EMITFSI (a) and EMIFSI (b) at 30°C.

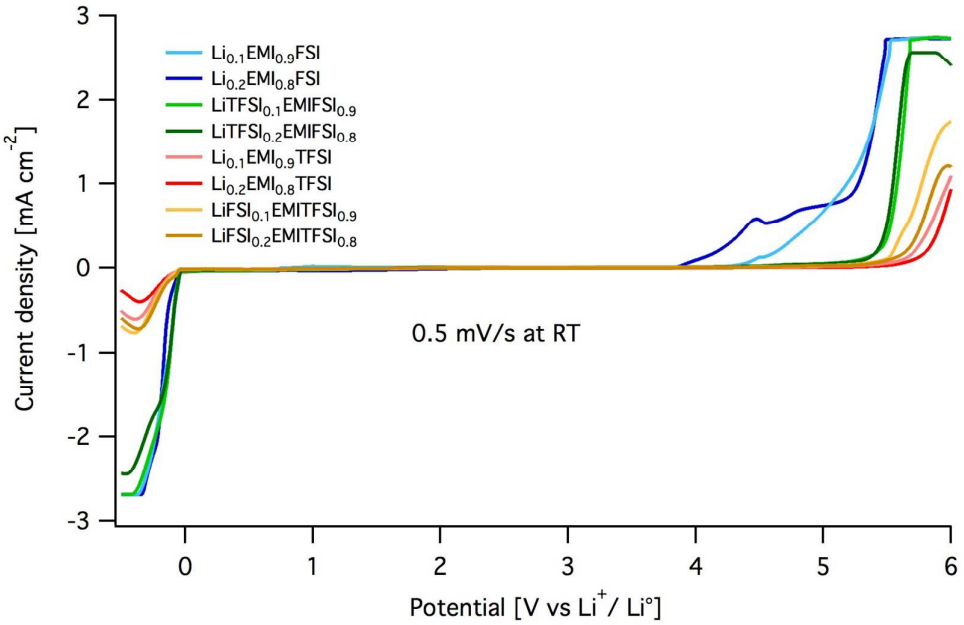

Figure 10: Voltammograms of the electrolytes from LSV at a scan rate of 0.5 mV s^{-1} between -0.5 and 6 V using stainless steel as the working electrode and Li-foil as the counter and reference electrode.